Acta Cryst. (1987). B43, 41-48

High-Resolution Electron Microscopy of Disordered Au–15at.%Mn Alloys

BY N. TANAKA* AND J. M. COWLEY

Department of Physics, Arizona State University, Tempe, AZ 85287, *USA*

AND K. OHSHIMA

Department of Applied Physics, Nagoya University, Nagoya 464, *Japan*

(*Received* 30 *December* 1985; *accepted* 24 *July* 1986)

Abstract

Quenched Au–15at.%Mn alloys are observed in the axial bright-field imaging mode along [001] and [0$\bar{1}$2] directions. The essence of the local structure is clarified in connection with the short-range-order (SRO) diffuse scattering. The micrographs and diffraction patterns do not show any features corresponding to small domains of the ordered phases. However, the micrographs, taken with the fundamental reflections and the SRO diffuse scattering at [001] incidence, show locally regular arrangements of black strips with antiphase relation. The arrangements are consistent with the distribution of the SRO diffuse scattering; they can be interpreted as reflections through a nonlinear projection of the three-dimensional linked structure of Mn atoms (chain structure) revealed previously by X-ray diffuse-scattering analysis. From the observations, a structural model is proposed in [001] projection, which can explain the distribution of the SRO diffuse scattering.

1. Introduction

The atomic structures of disordered binary alloys and their accompanying physical properties have been of interest since the original study of single-crystal Cu_3Au alloys showed pronounced short-range order (SRO) above the critical temperature (Cowley, 1950*a*). Quantitative analyses of the local structures in several disordered alloys have been carried out by X-ray diffraction (CuAu: Roberts, 1954; Metcalfe & Leake, 1975; $CuAu_3$: Batterman, 1957; Cu_3Au: Moss, 1964; Bardhan & Cohen, 1976; Cu-29·8at.%Pd: Ohshima, Watanabe & Harada, 1976; CuPt, Hashimoto & Iwasaki, 1979; Au_4Mn: Fürnrohr, Epperson & Gerold, 1980; Suzuki, Harada, Nakashima & Adachi, 1982). In these analyses, the two-body correlation functions, namely the SRO parameters, were obtained by measuring the intensity of the SRO diffuse scattering (Cowley, 1950*a*, *b*). On the other hand, electron diffraction patterns of disordered samples contain information about the many-body correlations of the constituent atoms through the dynamical diffraction effect. The multiple-correlation parameters including the SRO ones are hard to separate quantitatively in the diffraction intensity. To a good approximation, the multiple correlations can be expressed in terms of the 'dynamical factor' by which the kinematical diffraction intensity is multiplied (Fields & Cowley, 1978). This cannot, however, give phase information for the structural analysis.

Gehlen & Cohen (1965), using the SRO parameters of disordered Cu_3Au alloys, reconstructed the atomic arrangement by computer simulation. They inferred that the SRO structure consisted of small ordered domains with antiphase boundaries in the disordered matrix. Suzuki, Harada, Nakashima & Adachi (1982) reconstructed the three-dimensional atomic arrangement of quenched Au_4Mn alloys by using detailed SRO parameters and a dedicated simulation program. Their models for the structures are derived solely from the two-body correlation functions and are not necessarily unique given the fact that a limited set of input correlation functions is used. In principle, high-resolution electron microscopy provides an improved means for testing such structures in a reasonably representative volume, provided that the overlap problem can be solved.

Electron-microscopic observations of disordered binary alloys have been performed mostly with the tilted-illumination dark-field imaging mode. This method has been applied to disordered Cu_3Au (Yamaguchi, Watanabe & Ogawa, 1961; Sinclair & Thomas, 1975), Ni_4Mo (Ruedl, Delavignette & Amelinckx, 1968; Okamoto & Thomas, 1971), CuPt (Chevalier & Stobbs 1976), Au_4Cr (Dutkiewicz & Thomas, 1975), Cu-29·8at.% Pd and Cu-21·0at.% Pd (Tanaka, Ohshima, Harada & Mihama, 1979; Van Tendeloo & Amelinckx, 1983; Tanaka & Ohshima, 1984) alloys. The dark-field micrographs taken with the SRO diffuse scattering showed many bright speckles of a few nanometers in size suggesting the existence of ordered microdomains in the disordered samples. However, one of the present authors

* Present address: Department of Applied Physics, Faculty of Engineering, Nagoya University, Nagoya 464, Japan.

0108-7681/87/010041-08$01.50

(Cowley, 1973) pointed out the difficulty of image interpretation. The correspondence between the bright speckles and actual single ordered domains is not direct because of the overlap of domains and the dynamical diffraction effect. Recently, Chevalier & Stobbs (1979) and Chevalier & Craven (1977) studied quenched Cu-Pt alloys using the stereoimaging method in the dark-field mode and the microdiffraction technique in an attempt to overcome the overlap problem.

In the present paper, quenched Au-15at.% Mn alloys are observed in the axial bright-field imaging mode by the same procedure as described in the previous study of disordered Cu-Pd alloys (Tanaka & Ohshima, 1984). The Au-15at.% Mn composition was chosen for the following reasons: (i) the SRO parameters of quenched bulk Au-15at.% Mn alloys have been obtained in detail by X-ray diffraction and the atomic arrangement has been reconstructed through computer simulation (Ohshima, Harada, Matsui & Adachi, 1986), (ii) the diffuse scattering has been confirmed to be mainly due to the SRO of the constituent atoms by the Borie-Sparks (1971) method, and (iii) the quenched sample is expected to retain the SRO state above T_c because of the low T_c. The axial bright-field imaging mode is used because of the reliability of the image interpretation supported by established simulation methods. The result obtained from the images is compared with the local atomic arrangement reconstructed from the measured X-ray SRO parameters. Finally, approximate imaging theories to help to interpret the present results are briefly discussed.

2. Experimental

A single crystal of Au-15at.% Mn alloy was prepared from the melt in a high-purity alumina crucible by the Bridgman method. The materials were 99·99% gold and 99·9% manganese. The lattice parameter (a_0) of the crystal with the Bravais lattice of f.c.c. was found to be 0·407 nm by X-ray diffraction (Ohshima, Harada, Matsui & Adachi, 1986). The ingot was continuously homogenized under vacuum at 1223 K for one week. Sample slices of 3·0 mm in diameter and 0·2 mm in thickness were made from the ingot with the top surface parallel to either the (001) or $(0\bar{1}2)$ planes. The slices were then annealed at 773 K for three days in vacuum, quenched in ice brine, and electrolytically thinned for the microscopic observations using a mixed solution of water, hydrochloric acid and sulfuric acid (50 : 3 : 3 by volume) (Wolf, 1977).

The samples were observed in the bright-field imaging mode with [001] and $[0\bar{1}2]$ zone-axial illumination using a JEM-200CX microscope (accelerating voltage: $E = 200$ kV; spherical aberration coefficient of objective lens: $C_s = 1{\cdot}2$ mm) and using a JEM-4000EX microscope ($E = 350$ kV; $C_s = 1{\cdot}0$ mm). The $[0\bar{1}2]$ incidence is suitable for checking the existence of ordered Au_3Mn or Au_4Mn (Tanaka, Ohshima, Harada & Cowley, 1984). The bright-field micrographs were taken with (i) the direct beam and the SRO diffuse scattering, and (ii) the direct beam, the SRO diffuse scattering and the 200 and 220 fundamental reflections. The micrographs were analyzed using an optical diffraction apparatus with a He-Ne laser source ($\lambda = 6328$ Å) and an objective lens of focal length 0·9 m.

3. Results and interpretation

3.1. *Electron diffraction patterns at* [001] *incidence*

Fig. 1 shows an electron diffraction pattern of a quenched Au-15at.% Mn alloy taken at [001] incidence. The streaks between the fundamental spots are diffuse scattering due to the short-range order (SRO) of the constituent atoms. The diffuse maxima are also evident at the ends of streaks at, for example, $1,\frac{1}{4},0$ and $1,\frac{3}{4},0$ reciprocal points as indicated by arrows. For the same bulk sample, the distribution of the diffuse scattering agrees qualitatively with X-ray diffraction results as shown in Fig. 2 (Ohshima, Harada, Matsui & Adachi, 1986). The electron diffuse scattering is more evident and sharper than the X-ray diffuse scattering. Superstructure reflections as might be expected for ordered Au_4Mn or Au_3Mn are not observed in the diffraction pattern. The qualitative agreement between the X-ray and electron diffraction data demonstrates that the quenching procedure for the present thin Au-15at.% Mn sample was adequate even if this was not so for the Au_4Mn sample (Tanaka, Ohshima, Harada & Cowley, 1984), and the present results can appropriately be compared with those from X-ray diffraction.

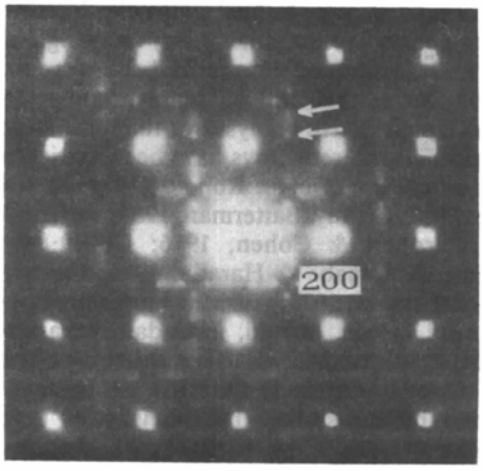

Fig. 1. Electron diffraction pattern of a quenched Au-15at.% Mn alloy at [001] incidence. Arrows indicate two intensity peaks in the SRO diffuse scattering.

3.2. *Electron-microscopic images at* [001] *incidence*

Figs. 3(*a*) and 3(*b*) show a pair of axial bright-field images of quenched Au–15at.%Mn alloys taken at [001] incidence with SRO diffuse scattering and with and without the 200 fundamental reflections, respectively. The image in Fig. 3(*a*) shows the 200 lattice fringes ($d = 2{\cdot}0$ Å) representative of the average periodic structure of the disordered sample (Cowley, 1981). The reason for the poor image contrast with the SRO diffuse scattering may be that the scattering intensity is 10^{-4} times weaker than the fundamental reflections measured in X-ray diffraction. The image in Fig. 3(*b*) shows locally fringe-like contrast tilted by an average of 15° from the [010] direction. We interpret the fringe contrast as having its origin in the SRO diffuse scattering which arises from deviations from the average periodic structure. The fringes are not well aligned over distances larger than about 2 nm as shown by the dotted circles. We infer from the angle of the fringes and the average spacing that the fringes are associated mainly with the diffuse maxima indicated by arrows in Fig. 1. This micrograph suggests that localized regular arrangements exist mainly in directions tilted by an average of 15° from the [100] or [010] directions when the SRO state is observed in the [001] direction in electron microscopy. The origin of the fringe contrast will be clarified later with reference to higher-resolution micrographs (Figs. 4*a* and 5*a*). It should be noted that the size of the two-dimensional arrangements in the image does not necessarily correspond to that of the actual three-dimensional localized ordering because of overlapping. The fringe contrast is relatively insensitive to sample thickness. The reason may be that, for disordered alloys, the difference in composition of neighboring columns is generally less than that for ordered alloys, so the effective extinction distance of SRO diffuse scattering may be much greater than that of superstructure or fundamental reflections.

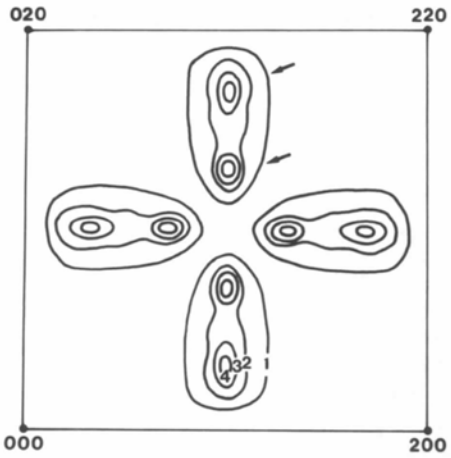

Fig. 2. Contour map of the SRO diffuse-scattering intensity of a quenched Au–15at.%Mn alloy measured in the X-ray diffraction pattern at [001] incidence.

Fig. 4(*a*) shows a high-resolution axial bright-field image taken near the optimum defocus with a JEM-4000EX microscope operated at an accelerating voltage of 350 kV. The image resolution at the extended

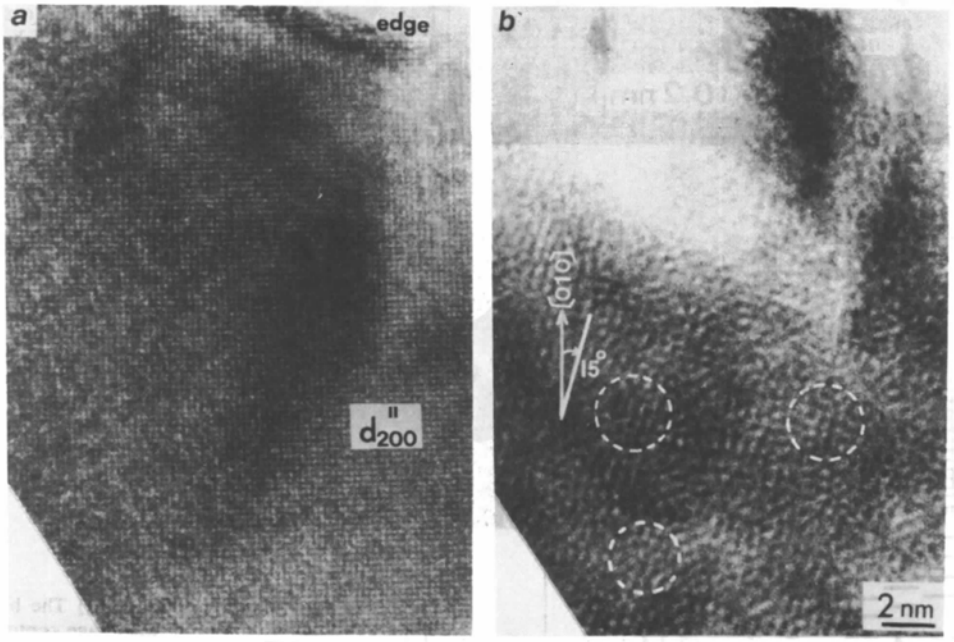

Fig. 3. Axial bright-field images of a quenched Au–15at.%Mn alloy taken with a JEM-200CX using (*a*) SRO diffuse scattering and 200 fundamental reflections, and (*b*) the diffuse scattering only at [001] incidence. White circles indicate the regular arrangements.

Scherzer defocus is expected to be 1·8 Å. The image was taken with the fundamental reflections and the SRO diffuse scattering. Fig. 4(*b*) is the optical diffraction pattern of the image. The pattern is essentially similar to the electron diffraction pattern in Fig. 1 within the spatial frequency of about $(2\,\text{Å})^{-1}$. The sample thickness in this region is estimated to be about 120 Å judging from the extinction of the 200 lattice fringes. In the micrograph, the 200 lattice fringes are observed in horizontal and vertical directions. Furthermore, several black strips ranging from 4 ($=a_0$) to 8 Å ($=2a_0$) are regularly arranged on the 200 lattice fringes with a separation of 4 Å ($=2d_{200}$) along the [100] or [010] directions. The arrangements are then stacked in antiphase relation along the [010] or [100] directions as indicated by white arrows. The contrast of the arrangements arises from the SRO diffuse scattering. The lateral size of the regular arrangements is typically 20–30 Å, although the value does not necessarily correspond to the actual size of the three-dimensional ordering. It has been checked whether the contrast of the strips is simply reversed by a change of defocus or a change of thickness. The typical arrangements of the strips are retained except for reversal of contrast at any thickness ranging from 100 to about 400 Å. Comparing the thickness insensitiveness of lattice-like fringes due to the SRO diffuse scattering in Fig. 3(*b*), the contrast reversal is caused

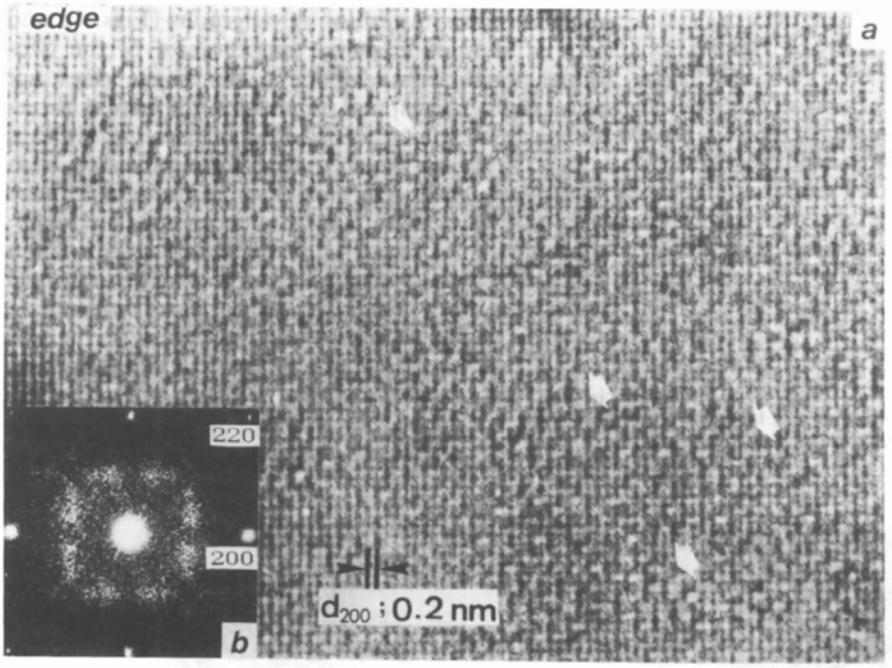

Fig. 4. High-resolution axial bright-field image of a quenched Au-15at.%Mn alloy taken with a JEM-4000EX at [001] incidence (*a*), and the optical diffraction pattern of the image (*b*). Arrows indicate the regular arrangements of black strips.

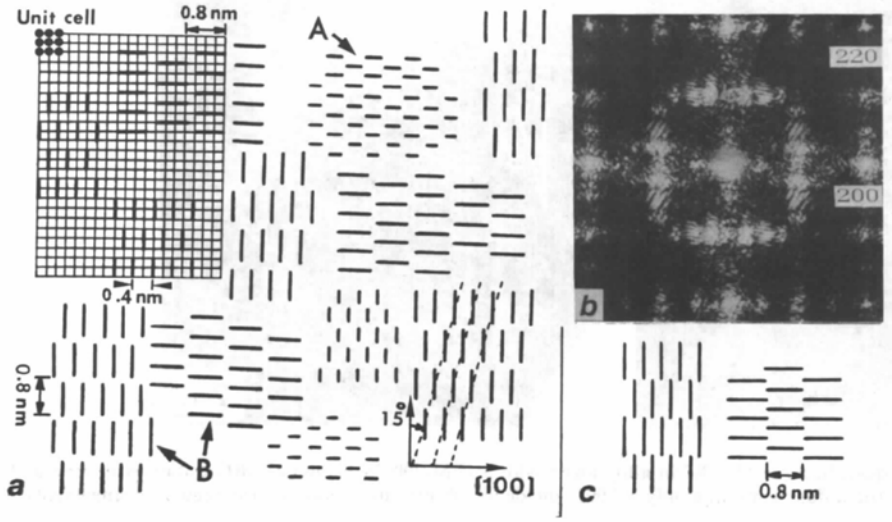

Fig. 5. (*a*) The best-fit model of the image contrast in Fig. 4(*a*), (*b*) the optical diffraction pattern of the model and (*c*) another type of model.

by modulation by 200 fundamental reflections. These results show that the arrangements reflect an essential structure existing in the sample in spite of dynamical diffraction effects.

3.3. *Interpretation of the image contrast*

In the interpretation of the image contrast, our first task is the identification of the geometry of the image contrast, the second is to check the transfer characteristic of the microscope for the wavefunction of imaging electrons from below the sample to the recording plane, and the third is to consider the relation between the wavefunction and the three-dimensional SRO structure of the sample.

Optical diffraction is useful for the first part of the interpretation. Fig. 5(*a*) is a model of the image contrast appearing in Fig. 4(*a*), and Fig. 5(*b*) is the optical diffraction pattern. The model is composed mainly of arrangements of strips with antiphase relation of the period of 8 Å, as indicated by arrows (*B*). The optical diffraction patterns in Figs. 4(*b*) and 5(*b*) are quite similar. This means that the model retains the essential feature of the image contrast in Fig. 4(*a*), although the model has a higher density of ordered arrangements than exhibited in the micrograph. Also, another type of arrangement (Fig. 5*c*) may exist locally, because it gives a similar optical diffraction pattern. The value, 8 Å, represents only an average value in a statistically continuous distribution of the length of the strips in the image.

For the second step, it is noted that the intensity distributions of the electron diffraction pattern in Fig. 1 and the optical diffraction pattern from the image in Fig. 4(*b*) are similar, and can be said to differ only by a slowly varying multiplicative function. The diffraction amplitudes may also differ by a similar slowly varying complex function as a first approximation. This difference may arise mainly from the lens-transfer function which varies slowly in the relevant range for an image resolution of 2 Å. The image intensity must be thus related to the wavefunction at the exit surface of the crystal by convolution with a highly localized, complex spread function. The exit wavefunction must therefore be modulated in a manner similar to the distribution as sketched in Fig. 5(*a*), which also shows the exit intensity distribution. The low-resolution micrograph of the intensity distribution gives the fringe-like contrast tilted by 15° from the [101] direction as shown in the lower right of Fig. 5(*a*). The fringes correspond to those described in Fig. 3(*b*).

Our third step is to relate an intensity distribution of the form of Fig. 5(*a*) to the SRO state of the crystal. Fig. 6 shows a local arrangement of Mn atoms in the quenched bulk Au-15at.%Mn alloy reconstructed from the measured SRO parameters by computer simulation (Ohshima, Harada, Matsui & Adachi, 1986). In the figure, only the first- and second-nearest neighbors of Mn atoms are connected by lines. The result shows that the Mn atoms tend to adopt chain-like arrangements of length a_0 ($=4$ Å), $2a_0$ or $3a_0$ along three ⟨100⟩ directions. Comparing Fig. 5(*a*) with Fig. 6, the geometrical correspondence suggests a tempting direct interpretation of the contrast in Fig. 5(*a*), although a full projection relation is obviously inapplicable.

Following the results of our more detailed investigation of the imaging of structures with small numbers of point defects without strain ('diluted alloys'), and information given in a paper by Marks (1984), the intensity distribution at the exit surface of the crystal approximates a nonlinear representation of the projection of the structure in the axial beam direction with a limited spatial resolution as a result of the addition of phase-related amplitudes and the square of the amplitude (Tanaka & Cowley, 1987). In the present case also, the intensity of each lattice point may not be linearly related to the number of Mn atoms, but may represent a relative richness of Mn atoms.

From the above correspondence between black contrast and relative richness of Mn atoms in atomic columns, we propose a tentative atomic model of the [001]-projected SRO state in the present Au-15at.%Mn alloy as shown in Fig. 7(*a*). Although the relative richness of Mn atoms in each atomic column may be different, the same black dots are used for convenience in the figure. The arrangements with another kind of antiphase boundary as indicated by arrows (*) may correspond to the arrangements of strips as shown in Fig. 5(*c*). A two-dimensional Fourier transform of the atomic model gives a diffuse-scattering pattern reasonably similar to that obtained by electron diffraction (Figs. 1 and 7*b*). This optical Fourier simulation is equivalent to the computer calculation for obtaining a 001 section pattern of kinematical diffuse-scattering intensity due to the relevant three-dimensional SRO state (deviations from

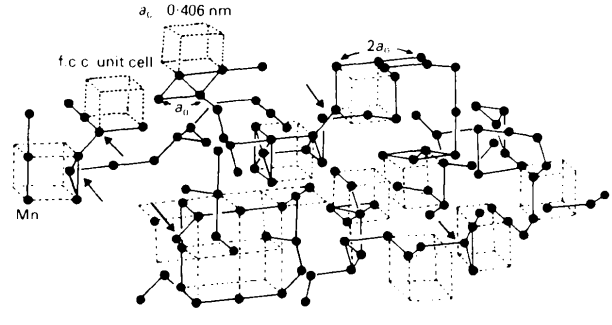

Fig. 6. Three-dimensional arrangements of Mn atoms in disordered Au-15at.%Mn alloys (basically, f.c.c. lattice) reconstructed by computer simulation using the SRO parameters obtained by X-ray diffraction. The first- and second-nearest-neighbor Mn atoms are connected by solid lines.

the averaged lattice), except for atomic-scattering factors.

In this model, the arrangements (A) with a strip length of 4 Å ($=a_0$) could explain the diffuse scattering at the $1,\frac{1}{2},0$ reciprocal point (arrow A in Fig. 7b). Other arrangements (B) with a length of 8 Å ($=2a_0$) could be responsible for the scattering at $1,\frac{1}{4},0$ and $1,\frac{3}{4},0$ reciprocal points (arrow B). A statistical discrete distribution of the chain length around the average values of 8 and 4 Å may cause the diffuseness. The diffuse maxima at $1,\frac{1}{4},0$ and $1,\frac{3}{4},0$ reciprocal points in the present X-ray and electron diffraction patterns suggest that the latter arrangement with a chain length of about $2a_0$ is dominant as a result of the projection in quenched Au-15at.%Mn alloys. In contrast, quenched Au-20at.%Mn alloys have both types of arrangement because of the additive diffuse maximum at the $1,\frac{1}{2},0$ reciprocal point (Suzuki, Harada, Nakashima & Adachi, 1982). Concerning the origin of the SRO diffuse scattering at $1,\frac{1}{2},0$, this was also recently discussed in detail by Van Tendeloo, Amelinckx & De Fontaine (1987) using optical models.

It should be stressed that the above model shows the essence of the local structure of the SRO state which gives the diffuse-scattering pattern in the form of a two-dimensional [001] projection. It is obviously hard to determine the full local atomic structure from this kind of one-electron micrograph.

3.4. *Electron-microscopic images at* [0$\bar{1}$2] *incidence*

Figs. 8(a) and 8(b) show a bright-field high-resolution image and the electron diffraction pattern taken at [0$\bar{1}$2] incidence. No superstructure reflections are seen in the diffraction pattern, although a pair of diffuse spots indicated by arrows (A) appear sharp. The spots are associated with the diffuse maxima as indicated by arrows in Fig. 1. The horizontal (B) and

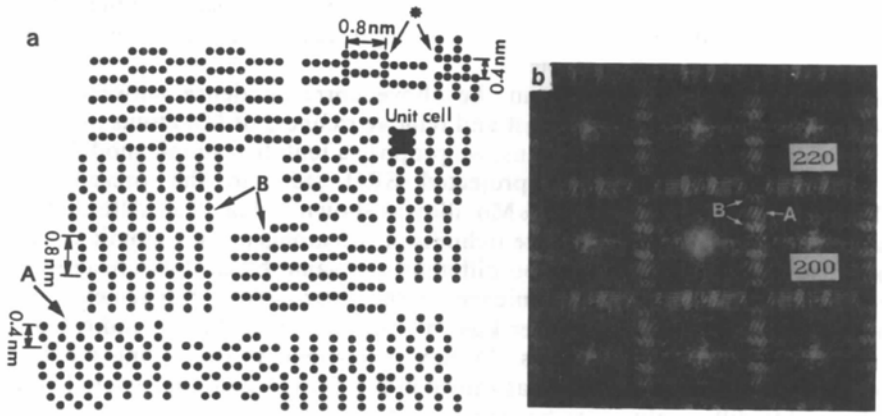

Fig. 7. (a) A two-dimensional [001]-projected structure model of Mn atoms in disordered Au-15at.%Mn alloys derived from the present observations and (b) the optical diffraction pattern. Arrows A and B indicate two types of regular arrangements and the corresponding diffuse scattering.

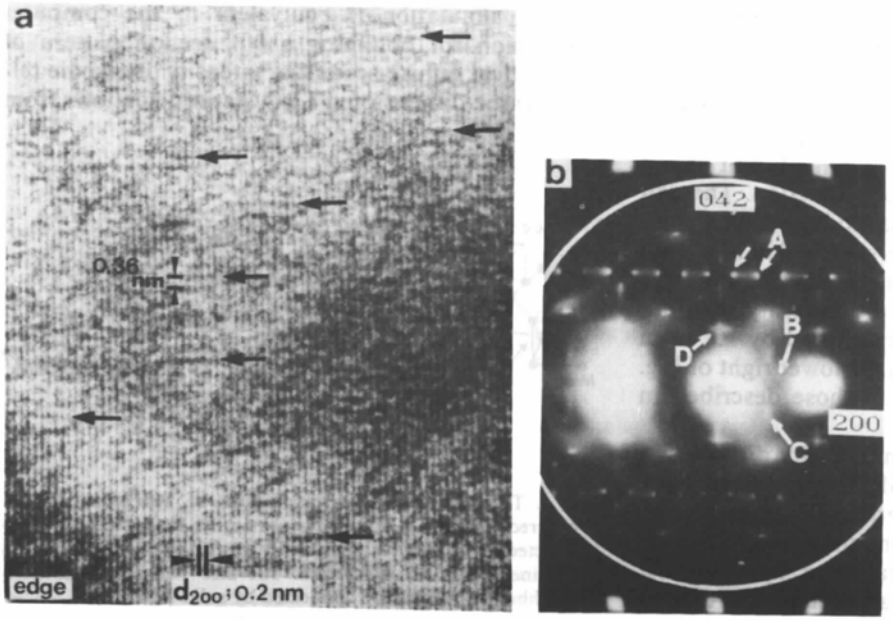

Fig. 8. (a) Axial bright-field image of a quenched Au-15at.%Mn alloy, and (b) the electron diffraction pattern at [0$\bar{1}$2] incidence. Arrows indicate irregular fringes of about 3·6 Å, which arise from the diffuse spot (D).

vertical (C) streaks are associated with the diffuse scattering connecting, for example, $1,\frac{1}{4},0$ and $1,\frac{3}{4},0$ reciprocal points in Fig. 1. They are not strongly excited in this incidence condition. The diffuse spot (D) arises from cutting the diffuse scattering extending along the [001] direction around the $0,1,\frac{1}{2}$ reciprocal point, as illustrated in Fig. 9(c). The point does not have a strong intensity in contrast with, for example, $0,1,\frac{1}{4}$ or $0,1,\frac{3}{4}$ reciprocal points in this alloy. The diffraction pattern agrees qualitatively with the $0\bar{1}2$ section of the three-dimensional distribution of the SRO diffuse scattering measured by X-ray diffraction.

In the micrograph, vertical fringes are lattice fringes resulting from the 200 fundamental reflections (d = 2·0 Å). Horizontal irregular fringes as indicated by arrows are due to the SRO diffuse scattering. These fringes have spacings between 3·5 and 3·7 Å and repeat by three to four spacings, although they are not well aligned over large distances along the [100] direction. This shows a heterogeneity of ordering as well as for the case at [001] incidence. An intuitive interpretation from the spacing suggests that the fringe contrast is associated with the $0,1,\frac{1}{2}$ period (d = 3·6 Å) of the diffuse spot (D) in Fig. 8(b). The period corresponds to the characteristic 'special point' Fourier harmonic for disordered Au-Mn alloys, as discussed before by Moss & Clapp (1968).

According to the model derived from the observations at [001] incidence, the diffraction intensity at the $1,\frac{1}{2},0$ reciprocal point, which is equivalent to the present $0,1,\frac{1}{2}$ point, is related to the regular arrangements with the strip length a_0 (A) in Fig. 7(a). The horizontal fringes are therefore a reflection of the local ordering with the a_0 unit in [0$\bar{1}$2] observation as marked by A in Figs. 9(a) and 9(b). In the figure, only local ordering oriented in one direction is depicted. The average length of the horizontal fringes shows the extent of the local ordering along the [100] direction, the value being 5–15 Å. Furthermore, repetition of the fringes indicates the extent of the local ordering along the [021] direction (Fig. 9b), although the overlap between different orderings should be taken into account. In this incidence condition, the fringes which reflect the local ordering with the $2a_0$ unit, as marked by B in Fig. 9(a), are not excited (d = 3·9 or 3·2 Å).

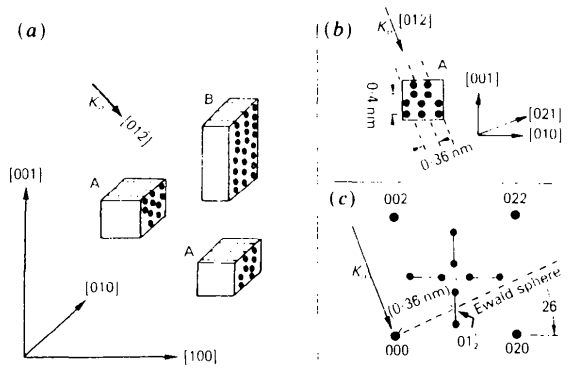

Fig. 9. (a), (b) Schematic drawings of the three-dimensional local ordering of Mn atoms and its observations along the [0$\bar{1}$2] direction, and (c) the 100 section of the distribution of the SRO diffuse scattering and Ewald sphere for [0$\bar{1}$2] incidence.

3.5. *Comparison between electron and X-ray results*

The present electron-microscopic observations suggest the relevance of the SRO diffuse scattering appearing at [001] incidence to linear arrangements of Mn-rich atomic columns with antiphase relation resulting from the [001] projection of three-dimensional structure as illustrated in Fig. 7(a). The structure is consistent with the essence of the local arrangements of quenched Au–15at.%Mn alloys revealed before by X-ray diffraction, namely a three-dimensional linked structure of Mn atoms (Fig. 6). However, an apparent difference in the size of the regular arrangements is detected: the electron micrographs taken along the [001] direction show relatively large ordered regions, where three or four strips are arranged along the [100] or [010] directions and the arrangements are stacked in two or three layers along the [010] or [100] directions. The atomic arrangements obtained by X-ray diffraction and computer simulation do not show such a strong localized ordering. This conflict may be due to the overlap effect in electron microscopy. Incidentally, the electron micrographs taken along the [0$\bar{1}$2] direction give another side view of the local ordering; the lateral size along the [100] direction is about 10 Å as indicated in Figs. 8 and 9. The image with large ordered regions in Fig. 4(a) may be formed by a 'coherent' addition of several small regular arrangements located at different depths along the [001] direction. One of the reasons for the coherent addition will be discussed briefly later. Furthermore, the existence of antiphase boundaries is not clear in Fig. 6, because the measured X-ray diffuse scattering does not have strong and sharp diffuse maxima, for example, at the $1,\frac{1}{4},0$ and $1,\frac{3}{4},0$ reciprocal points as appearing in an electron diffraction pattern such as that of Fig. 1. This suggests that electron microscopy and diffraction may accentuate the existence of antiphase boundaries by some effects including overlapping due to projection from three to two dimensions.

4. Discussion

In the present high-resolution electron micrographs taken at [001] incidence, the linear arrangements of relatively Mn-rich atomic columns mentioned in Fig. 7(a) appear as strips with white or black contrast (Fig. 4a). The reason why the individual atomic columns are not resolved may be a slight tilt of the sample from the [001] zone axis and effectively

reduced contrast transfer from 1·8 to more than 2·0 Å. Furthermore, the strips appear more stongly along the vertical direction than the horizontal direction. The result is also due to a slight tilt from the axial condition.

We note again that the above contrast of the strips comes from a nonlinear projection of three-dimensional linked structures of Mn atoms. The atomic arrangement at the antiphase boundaries in Fig. 7(*a*) may also be a result of the projection. The present observations show only the existence of linked Mn atoms and the antiphase relations between them, which can explain reasonably the SRO diffuse scattering. The images of disordered Au-15at.% Mn show the characteristic features of the SRO state obtained by X-ray diffraction, as if a projection approximation would hold. The explanation of the result may be found around imaging theories based on a kind of atomic-column approximation (Van Dyck, Van Tendeloo & Amelinckx, 1982; Marks, 1984) as follows: (i) the wave intensity at an atom position below a sample is approximately determined only by the relative composition in the atomic column just above it, although the relation is nonlinear; (ii) one-to-one correspondence between the wavefunction below the sample and the image intensity is required [localization of imaging (Marks, 1985)]. For the first point, the validity for f.c.c. crystals composed of one type of heavy atom such as gold has been mentioned in terms of a channeling effect by Marks (1984). Checking on the validity for gold crystals with small numbers of deviations, such as point defects, shows that the channeling effect simplifies the image formation in a limited image resolution larger than about 3 Å for gold-rich alloys (Tanaka & Cowley, 1987).

With the above conditions satisfied, the short-range ordering located at different depths along the *z* direction may be projected coherently, preserving characteristic spacings and lattice relations, when the columns are separated by more than about 3 Å and the alloy is 'diluted'. The general features of the SRO state rather than the full local atomic structure in disordered samples could be revealed by high-resolution electron microscopy using SRO diffuse scattering as a complementary method to X-ray diffraction. The observations along one crystallographic direction may, however, be misleading as regards the extent of the ordering. Detailed comparison of the size distribution with results from X-ray diffraction needs observations of the same area along various crystallographic directions together with the relevant simulations, which should be supported also by other dark-field imaging methods (Stobbs, 1984).

The authors express sincere thanks to Professor J. Harada of Nagoya University for suggesting this topic and for valuable discussions, Professor S. C. Moss of Houston University for crucial discussions and checking the manuscript, Dr D. Shindo of Tohoku University for illuminating discussions, Professor K. Mihama of Nagoya University for encouragement through the present study, and Dr J. Barry for help in the microscope operations. The study was supported by NSF grant DMR 7926460 and performed using the facility for high-resolution electron microscopy at Arizona State University.

References

BARDHAN, P. & COHEN, J. B. (1976). *Acta Cryst.* A**32**, 597-614.
BATTERMAN, B. W. (1957). *J. Appl. Phys.* **28**, 556-561.
BORIE, B. & SPARKS, C. J. (1971). *Acta Cryst.* A**27**, 198-201.
CHEVALIER, J. P. & CRAVEN, A. J. (1977). *Philos. Mag.* **36**, 67-79.
CHEVALIER, J. P. & STOBBS, W. M. (1976). *Electron Microscopy*, Vol. 1, edited by D. BRANDON, pp. 515-517. Jerusalem: Tal International.
CHEVALIER, J. P. & STOBBS, W. M. (1979). *Acta Metall.* **27**, 285-299.
COWLEY, J. M. (1950*a*) *J. Appl. Phys.* **21**, 24-30.
COWLEY, J. M. (1950*b*). *Phys. Rev.* **77**, 669-675.
COWLEY, J. M. (1973). *Acta Cryst.* A**29**, 537-540.
COWLEY, J. M. (1981). *Diffraction Physics*, 2nd ed., ch. 7. Amsterdam: North-Holland.
DUTKIEWICZ, J. & THOMAS, G. (1975). *Metall. Trans.* **6A**, 1919-1928.
FIELDS, P. M. & COWLEY, J. M. (1978). *Acta Cryst.* A**34**, 103-112.
FÜRNROHR, P., EPPERSON, J. E. & GEROLD, V. (1980). *Z. Metallkd.* **71**, 403-409.
GEHLEN, P. C. & COHEN, J. B. (1965). *Phys. Rev. A*, **139**, 844-855.
HASHIMOTO, S. & IWASAKI, H. (1979). *Phys. Status Solidi A*, **51**, 673-682.
MARKS, L. D. (1984). *Surf. Sci.* **139**, 281-298.
MARKS, L. D. (1985). *Ultramicroscopy*, **18**, 33-38.
METCALFE, E. & LEAKE, J. A. (1975). *Acta Metall.* **23**, 1135-1143.
MOSS, S. C. (1964). *J. Appl. Phys.* **35**, 3547-3553.
MOSS, S. C. & CLAPP, P. C. (1968). *Phys. Rev.* **171**, 764-777.
OHSHIMA, K., HARADA, J., MATSUI, M. & ADACHI, K. (1986). *J. Magn. Magn. Mater.* **54-57**, 157-158.
OHSHIMA, K., WATANABE, D. & HARADA, J. (1976). *Acta Cryst.* A**32**, 883-892.
OKAMOTO, P. R. & THOMAS, G. (1971). *Acta Metall.* **19**, 825-841.
ROBERTS, W. (1954). *Acta Metall.* **2**, 597-603.
RUEDL, E., DELAVIGNETTE, P. & AMELINCKX, S. (1968). *Phys. Status Solidi*, **28**, 305-328.
SINCLAIR, R. & THOMAS, G. (1975). *J. Appl. Cryst.* **8**, 206-210.
STOBBS, W. M. (1984). *J. Microsc. (Oxford)*, **136**, 137-151.
SUZUKI, H., HARADA, J., NAKASHIMA, T. & ADACHI, K. (1982). *Acta Cryst.* A**38**, 522-529.
TANAKA, N. & COWLEY, J. M. (1987). *Acta Cryst.* In preparation.
TANAKA, N. & OHSHIMA, K. (1984). *Phys. Status Solidi A*, **81**, 129-138.
TANAKA, N., OHSHIMA, K., HARADA, J. & COWLEY, J. M. (1984). *Proc. 42nd EMSA*, edited by G. W. BAILEY, pp. 426-427. San Francisco Press.
TANAKA, N., OHSHIMA, K., HARADA, J. & MIHAMA, K. (1979). *AIP Conf. Proc.* **53**, 292-293.
VAN DYCK, D., VAN TENDELOO, G. & AMELINCKX, S. (1982). *Ultramicroscopy*, **10**, 263-280.
VAN TENDELOO, G. & AMELINCKX, S. (1983). *Phys. Status Solidi A*, **77**, K9.
VAN TENDELOO, G., AMELINCKX, S. & DE FONTAINE, D. (1987). *Acta Cryst.* In preparation.
WOLF, R. (1977). *Micron*, **8**, 171-172.
YAMAGUCHI, S., WATANABE, D. & OGAWA, S. (1961). *J. Phys. Soc. Jpn*, **17**, 1030-1041.